Respiratory Research

RESEARCH

Open Access

Intraluminal chloride regulates lung branching morphogenesis: involvement of PIEZO1/PIEZO2

Ana N. Gonçalves[1,2], Rute S. Moura[1,2], Jorge Correia-Pinto[1,2,3] and Cristina Nogueira-Silva[1,2,4*]

Abstract

Background Clinical and experimental evidence shows lung fluid volume as a modulator of fetal lung growth with important value in treating fetal lung hypoplasia. Thus, understanding the mechanisms underlying these morphological dynamics has been the topic of multiple investigations with, however, limited results, partially due to the difficulty of capturing or recapitulating these movements in the lab. In this sense, this study aims to establish an ex vivo model allowing the study of lung fluid function in branching morphogenesis and identify the subsequent molecular/ cellular mechanisms.

Methods Ex vivo lung explant culture was selected as a model to study branching morphogenesis, and intraluminal injections were performed to change the composition of lung fluid. Distinct chloride (Cl^-) concentrations (5.8, 29, 143, and 715 mM) or Cl^- channels inhibitors [antracene-9-carboxylic acid (A9C), cystic fibrosis transmembrane conductance regulator inhibitor172 (CFTRinh), and calcium-dependent Cl^- channel inhibitorA01 (CaCCinh)] were injected into lung lumen at two timepoints, day0 (D0) and D2. At D4, morphological and molecular analyses were performed in terms of branching morphogenesis, spatial distribution (immunofluorescence), and protein quantification (western blot) of mechanoreceptors (PIEZO1 and PIEZO2), neuroendocrine (bombesin, ghrelin, and PGP9.5) and smooth muscle [alpha-smooth muscle actin (α-SMA) and myosin light chain 2 (MLC2)] markers.

Results For the first time, we described effective intraluminal injections at D0 and D2 and demonstrated intraluminal movements at D4 in ex vivo lung explant cultures. Through immunofluorescence assay in in vivo and ex vivo branching morphogenesis, we show that PGP9.5 colocalizes with PIEZO1 and PIEZO2 receptors. Fetal lung growth is increased at higher [Cl^-], 715 mM Cl^-, through the overexpression of PIEZO1, PIEZO2, ghrelin, bombesin, MLC2, and α-SMA. In contrast, intraluminal injection of CFTRinh or CaCCinh decreases fetal lung growth and the expression of PIEZO1, PIEZO2, ghrelin, bombesin, MLC2, and α-SMA. Finally, the inhibition of PIEZO1/PIEZO2 by GsMTx4 decreases branching morphogenesis and ghrelin, bombesin, MLC2, and α-SMA expression in an intraluminal injection-independent manner.

Conclusions Our results identify PIEZO1/PIEZO2 expressed in neuroendocrine cells as a regulator of fetal lung growth induced by lung fluid.

Keywords Chloride, Branching, Lung development, Lung fluid, Mechanotransduction

*Correspondence:
Cristina Nogueira-Silva
cristinasilva@med.uminho.pt
[1] School of Medicine, Life and Health Sciences Research Institute (ICVS), University of Minho, Campus de Gualtar, Gualtar, 4710-057 Braga, Portugal
[2] Life and Health Sciences Research Institute/3B's-PT Government Associate Laboratory, Braga/Guimarães, Portugal
[3] Department of Pediatric Surgery, Hospital de Braga, Braga, Portugal
[4] Department of Obstetrics and Gynecology, Hospital de Braga, Braga, Portugal

Background

Physical forces exerted on the developing fetal lung, namely by intraluminal lung fluid and peristaltic airway contractions, are important regulators of fetal lung branching morphogenesis. Lung fluid and its in utero intraluminal hydraulic pressure have two sources: amniotic fluid and secretions of the epithelial cells into the airway lumen, which are osmotically driven by active chloride (Cl^-) secretion through Cl^- channels; this gives rise to a continuous forward flow of lung liquid that drains into the amniotic fluid. The physiological circulation of lung fluid filling the air spaces is critical to lung development. In fact, if it is disturbed, lung growth and maturation are impaired. For instance, excess fluid drainage during fetal life or a decrease of fluid pressure due to premature rupture of the membranes or oligohydramnios are associated with lung hypoplasia with underbranched lungs, which is a major cause of respiratory insufficiency and mortality in newborns [1–8]. In opposition, experimental evidence shows the increase of lung fluid volume as a promotor of fetal lung growth [2, 9]. In fact, prenatal tracheal occlusion increases lung fluid volume, luminal pressure, and expansion and, consequently, enhances the branching rate [5, 10–13]. This evidence allowed the development of fetoscopic endoluminal tracheal occlusion (FETO) as a treatment for the more severe cases of pulmonary hypoplasia in the context of congenital diaphragmatic hernia (CDH) [13–16].

Molecular studies have been performed to determine the mechanisms underlying lung fluid production and pulmonary expansion. In brief, the lung fluid is produced by a mechanism dependent on sodium–potassium adenosine triphosphatase (Na^+/K^+-ATPase) pumps and $Na^+/K^+/2$chloride (Cl^-) co-transporters located on the basolateral surface of pulmonary epithelial cells [17–21], that stimulate the apical Cl^- secretion via cystic fibrosis transmembrane conductance regulator (CFTR) or calcium-dependent chloride channel (CaCC). Finally, it is the increase of intraluminal Cl^- concentration ($[Cl^-]$) that favors the movement of sodium and water into the lumen and promotes lung liquid formation and the consequent pulmonary expansion [5, 18–25]. In addition, inhibition of apical ionic channels, such as CFTR, transmembrane protein 16A (TMEM16A), chloride channel2 (ClC2), or the extracellular calcium receptor (CaR), induces key morphological defects in branching morphogenesis [18, 20, 26–30].

Recently, an emergent area, mechanotransduction, showed that cells are able to translate a mechanical stimulus, like pressure, into biochemical signaling. However, the mechanisms by which pressure is sensed in the lung have not been determined yet. In the fetal lung, smooth muscle cells are essential for peristaltic airway contractions, while the pulmonary neuroendocrine cells (PNECs)/ neuroepithelial bodies (NEBs) are indicated as chemo- and mechano-sensors, particularly during the perinatal period. Indeed, the peristaltic airway contractions generate not only the flow of intraluminal fluid but also the periodic distension and relaxation of the end buds essential for branching morphogenesis [31–34]. Oppositely, PNECs/NEBs are promotors of in vivo and ex vivo fetal lung growth [35–39] and sensors for hypoxia, hypercapnia, acidosis, or airway stretch [40] with undefined functions in fetal lung development. A recent publication showed that PIEZO2, a known mechanosensor [41–43], is expressed in NEBs, indicating that NEBs can sense mechanical stretch [41]. This study also reports the presence of PIEZO2 in sensory neurons and its importance in regulating lung expansion and efficient neonatal respiration in a mechanism dependent on the central nervous system [41]. However, the inactivation of PIEZO2 in sensory neurons, but not in PNECs/NEBs, was essential for respiratory transition at birth [41], maintaining the importance of stretch sensation by PNECs unclear.

PIEZO proteins, PIEZO1 and PIEZO2, are mechanically activated cation channels that form homomultimeric complexes sufficient to mediate mechanically induced currents [44–46]. Previous work showed PIEZO1 as essential in the regulation of basal blood pressure and normal cellular volume in red blood cells in adulthood [43, 47], whereas PIEZO2 mediated the sensory processes [48–50] and the respiratory physiology [41].

In this context, to investigate the mechanotransduction signaling intrinsic to fetal lung growth, we explore the neuroendocrine cells and the mechanoreceptors as mediators of intraluminal fluid composition during branching morphogenesis.

Methods

Animals

Female Sprague–Dawley rats (225 g; Charles-River; Spain) were maintained in appropriate cages under controlled conditions and fed with commercial solid food. The rats were mated and checked daily for vaginal plug. The day of plugging was defined as embryonic day (E) 0.5 for time dating purposes. Embryos were dissected at E13.5 or E17.5, and the embryonic lungs were removed for further analysis.

Lung explant cultures

Harvesting and dissection of E13.5 lungs were made in PBS under a dissection microscope (Leica MZFLIII, Switzerland). Lungs were then transferred to the nucleopore membranes (Cat No. TETP01300, Whatman, USA) and cultured in a complete medium [50% DMEM low

glucose, 50% nutrient mixture F-12 (Gibco, USA) supplemented with 100 µg/mL glutamine (Cat. No. 25030081, Gibco, USA), 100 units/mL penicillin–streptomycin, (Cat. No. 15140122, Gibco, USA), 0.25 mg/mL L-ascorbic acid (Cat No. A4403, Sigma-Aldrich, USA) and 10% fetal bovine serum (FBS) (Cat No. 26140079, Gibco, USA)] [51]. The fetal lung explants were incubated in a 5% CO_2 incubator at 37 °C for 96 h, and the medium was replaced every 48 h. Explants were processed for immunofluorescence or western blot assay.

Lung fluid manipulation

Distinct chloride concentration

According to in vivo [23] and ex vivo [20, 52, 53] studies, 143 mM Cl^- was defined as basal [Cl^-]. The intraluminal [Cl^-] manipulation was achieved using three experimental concentrations: 5.8, 29, and 715 mM Cl^-. Lungs were randomly assigned to one of four experimental groups ($n \geq 12$ per condition). After intraluminal injections at day 0 (D0) and D2, morphological and molecular dynamics were determined at D4.

To strictly manipulate the [Cl^-] maintaining a similar concentration of the remaining ions, the following chemical compounds were used: potassium chloride (KCl, Cat No. 7447-40-7, Merck, Germany), magnesium chloride ($MgCl_2$, Cat No. 7786-30-3, Merck, Germany), calcium chloride ($CaCl_2$, Cat No. C1016-100G, Sigma-Aldrich, USA), potassium D-Gluconate (Cat No. G8270-100G, Sigma-Aldrich, USA), $MgSO_4$ (Cat No. M7506 Sigma-Aldrich, USA) and calcium D-gluconate (Cat No. C8231-100G, Sigma-Aldrich, USA). Specifically, KCl, $MgCl_2$, and $CaCl_2$ were used as donors of Cl^-, K^+, Mg^{2+}, and Ca^{2+}, while potassium D-gluconate, $MgSO_4$, and calcium D-gluconate worked as replace compounds as demonstrated in the Additional file 1: Table S1a, b. Thus, the relative influence of the different chemical compounds for the lower and higher [Cl^-] were as follow (in mM, adapted from [54]): 5.8 mM Cl^-: KCl (5.711), $MgCl_2$ (0.049), $CaCl_2$ (0.041), D-glucose (10.000, Cat No. G8270-1KG, Sigma-Aldrich, USA), HEPES (5.000, Cat No. H3375-25G, Sigma-Aldrich, USA), potassium D-gluconate (698.290), $MgSO_4$ (5.950, Cat No. M7506-1KG-M, Sigma-Aldrich, USA), Calcium D-gluconate (4.960, Cat No. C8231-100G, Sigma-Aldrich, USA); 715 mM Cl^-: KCl (704.000), $MgCl_2$ (6.000), $CaCl_2$ (5.000), D-glucose (10.000), HEPES (5.000) as shown in Additional file 1: Table S1a, b.

Chloride channel inhibitors

Anthracene-9-carboxylic acid (A9C, Cat No. A89405, Sigma-Aldrich, USA) (Valenzuela et al., 2000; Al Khamici et al., 2015), CFTRinh (Cat No. C2992, Sigma-Aldrich, USA) (Li et al., 2007; Melis et al., 2014) or calcium-dependent Cl^- channel inhibitor A01 (CaCCinh, Cat No. SML0916, Sigma-Aldrich, USA) (Boedtkjer et al., 2015; Nakazawa et al., 2016) were dissolved in dimethyl sulfoxide (DMSO, Cat No. D8418, Sigma-Aldrich, USA) according to the manufacture's protocol guidelines. Lung explants were randomly assigned to one of four experimental groups: A9C (10 µM), CFTRinh (5 µM), CaCCinh (10 µM), or matching volumes of DMSO for control ($n \geq 12$ per condition).

Inhibitors and DMSO were diluted in a standard solution containing (in mM): sodium chloride (135.000, NaCl, Cat No. 7647-14-5, Merck, Germany), KCl (5.000), $MgCl_2$ (1.200), $CaCl_2$ (1.000), D-glucose (10.000), HEPES (5.000) were used as vehicle according to the previously published work adapted from [20].

Intraluminal injections

Pulmonary tissues were punctured for intraluminal injections. For that, borosilicate glass capillaries (1.55 mm outer diameter, 1.15 mm inner diameter; HIRS9201590, VWR International, USA) were pulled using Flaming Brown Micropipette Puller (P500, Heat 545, Vel 13, Del 10; Model P-97, Sutter Instrument Co., USA). Lung explants were randomly selected and, under the stereoscopic dissecting microscope (Olympus SZX16 stereomicroscope), the intraluminal injections were performed on day0 (D0) and day2 (D2). The pulled borosilicate glass capillary was filled with one of the experimental solutions marked with trypan blue (Cat No. T8154, Sigma-Aldrich, USA), and the capillary was then slowly inserted into the lumen. The presence of trypan blue in the lumen was indicative of a successful procedure. Only the lung explants with effective injections at D0 and D2 and perfectly placed in the nucleopore membrane were considered for analysis.

PIEZO1/PIEZO2 inhibition

GsMTx4 (Cat No. ab141871, Abcam, UK), a selective PIEZO1/PIEZO2 inhibitor, was diluted in water. At the final concentration of 5 µM, GsMTx4 was added to the culture medium on the day of intraluminal injections, D0 and D2, in accordance with the previously published work [42, 55, 56]. Lungs were randomly assigned to one of four experimental groups ($n \geq 12$ per condition).

Morphometric analysis

The branching morphogenesis was monitored daily by photographing the explants. At D0 (0 h) and D4 (96 h) of culture, the branching of all lung explants was determined by counting the number of peripheral airway epithelial buds of the developing respiratory tree [57]. For the morphometric analysis, the internal perimeter of the lung (epithelium) was assessed at D0 and D4 using Axion-Vision Rel 4.3 (Carl Zeiss GmbH, Germany).

Immunofluorescence

For immunostaining, lungs at E17.5 and from the lung explant cultures at D4 were fixed in 4% paraformaldehyde for 2 h or 15 min, respectively. Whole lungs and explants were then embedded in OCT (OCT compound, Cat No. 4582, Scigen, UK), sectioned (4 µm), and placed on SuperFrost®Ultra Plus slides (11976299, Thermo Scientific, UK).

Double immunostained using a 3-day protocol was performed (adapted from [58, 59]). Slides were first boiled in 10 mM citrate buffer (Cat No. AP-9003-125, Thermo Scientific, UK) for 20 min (in vivo samples) or 5 min (explant). Samples were blocked by incubation in 20% bovine serum albumin (Cat No. A3294, Sigma-Aldrich, USA) and 0.5% Triton X-100 (Cat No. 9036-19-5, Merck, Germany) for 4 h, followed by 36 h of incubation with primary antibodies at room temperature (RT). Sections were then washed and incubated with the corresponding secondary antibodies for 12 h in 1% BSA in PBS at RT. Finally, samples were washed in PBS1x, incubated with 4′,6-diamidino-2-phenylindole (DAPI, Cat No. D1306, Life Technologies, USA) for 1 min at RT, and mounted in PermaFluor™ Aqueous Mounting Medium (Cat No. TA-006-FM, Life Technologies, USA). Visualization and image capture of immunofluorescence staining was performed using an Olympus Widefield Upright Microscope BX61 (Olympus Corporation, Japan).

The primary antibodies used were PGP9.5 (1:150, Cat No. ab72911, Abcam, UK), PIEZO1 (1:50, Cat No. NBP1-78537, Novus Biologicals, USA), and PIEZO2 (1:50, Cat No. NBP1-78624, Novus Biologicals, USA). Negative control reactions included the omission of the primary antibody. The secondary antibodies were: Alexa Fluor 647-conjugated donkey anti-rabbit IgG(H + L) (1:500, Cat No. A31573, Life Technologies, USA) and Alexa Fluor plus 488-conjugated goat anti-mouse IgG(H + L) (1:500, Cat No. A32723, Life Technologies, USA). Different and unrepeated in vivo samples or lung explants were randomly selected, $n \geq 4$ per stage or condition/antibody.

Western blot

Lungs explants were processed for western blot analysis according to the previously described methods [51]. In brief, 15 µg of protein were loaded onto 10% acrylamide mini gels, electrophoresed at 100 V at room temperature, and then transferred to nitrocellulose membranes (HybondTM-C Extra, GE Healthcare Life Sciences, UK). Blots were blocked in 5% bovine serum albumin and probed with primary antibodies to ghrelin (1:250, ON, 4 °C; Cat No. sc10368, Santa Cruz Biotechnology Inc., USA), bombesin (1:250, ON, 4 °C; Cat No. H00002922-MO3, Novus Biologicals, USA), PIEZO1 (1:250, ON, 4 °C; Cat No. HPA047185, Sigma-Aldrich, USA), PIEZO2 (1:250, ON, 4 °C; Cat No. HPA040616, Sigma-Aldrich, USA), myosin light chain 2 (MLC2, 1 : 250; ON, 4 °C; Cat No. #3672, Cell Signaling Technology Inc., USA), and alpha-smooth muscle actin (α-SMA, 1:500, ON, 4 °C; Cat No. NBP2-33006, Novus Biologicals, USA) according to the manufacturer's instructions. For loading control, blots were probed with GAPDH (1 : 5000; Cat No. MAB5718, R&D system, USA). After this, membranes were incubated with the corresponding secondary antibodies, developed with Clarity West ECL substrate (Cat No. 1705060, Bio-Rad, USA), and the chemiluminescent signal was captured by the Chemidoc XRS (Bio-Rad, USA) [51].

Quantitative analysis was performed with Quantity One 4.6.5 1-D Analysis Software (Bio-Rad, USA). Three independent experiments were performed ($n \geq 4$ were used per antibody/condition).

Statistical analysis

All quantitative data are presented as mean ± standard deviation (SD). One-way ANOVA was performed for the number of peripheral airway buds, epithelial perimeter, and protein expression levels on [Cl^-] (5.8, 29, 143, 715 mM), and Cl^- channels inhibitors (SS, A9C, CFTRinh, CaCCinh). Two-way ANOVA was used in the analysis of both morphological (number of peripheral airway buds, epithelial perimeter) and the molecular (protein expression levels) effect after GsMTx4 exposure. The parametric test assumptions were previously verified, and an additional LSD test was used for post-test analysis. Statistical analysis was performed using the statistical software IBM SPSS Statistics 26.0. Statistical significance was confirmed at $p < \mu 0.05$, $\gamma 0.01$, $\beta 0.001$, and $\alpha 0.0001$.

Results

Intraluminal injection in ex vivo lung explant cultures

To establish the intraluminal injections in ex vivo lung explant cultures, lung tissue was punctured using pulled borosilicate glass capillaries, and, for the first time, effective intraluminal injections at D0 and D2 were performed, as demonstrated in the Additional file 1: Movie S1, and Additional file 2: Movie S2, respectively. Furthermore, dynamic luminal movements were observed at D4 (an additional movie file shows this in more detail, see Additional file 3: Movie S3) that recognized the existence of fetal lung liquid in ex vivo lung explant cultures.

Luminal chloride as a modulator of branching morphogenesis

To study the role of intraluminal composition in branching morphogenesis, ex vivo lung explants were cultured for 4 days after injection of distinct [Cl^-]: 5.8, 29,

143, 715 mM Cl^- or Cl^- channels inhibitors: SS, A9C, CFTRinh, CaCCinh.

Morphometric analysis revealed an opposite effect in branching morphogenesis after injection of 5.8 and 715 mM Cl^-, indicated by the ratio of D4 and D0 in the number of peripheral airway buds (Fig. 1a, b) and epithelial perimeter (Fig. 1c). Specifically, when compared to basal [Cl^-], 5.8 mM inhibits, whereas 715 mM Cl^- stimulates both the number of peripheral airway buds (Fig. 1b) and the epithelial perimeter (Fig. 1c). Unexpectedly, 29 mM injection did not change branching morphogenesis at D4 compared to basal, 143 mM Cl^- (Fig. 1a–c).

Regarding the Cl^- channels inhibitors, an important inhibitory effect in terms of the number of peripheral airway buds (Fig. 1d–e) and epithelial perimeter (Fig. 1f) was visualized after CFTRinh or CaCCinh injections when compared with SS, while unchanged lung growth was observed after A9C luminal injection (Fig. 1d–f).

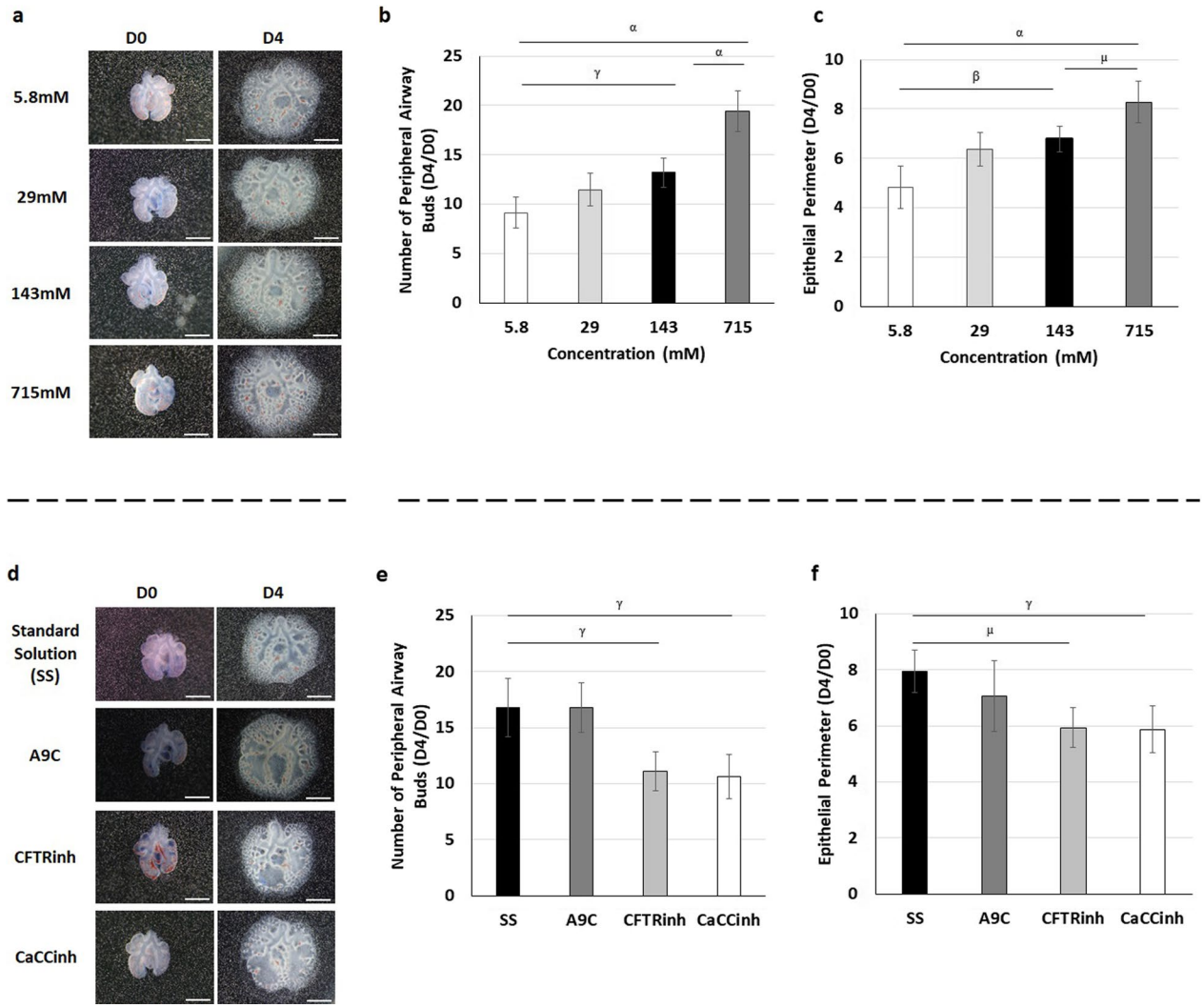

Fig. 1 Intraluminal chloride modulates branching morphogenesis. Upper panel: **a** represents lung explants on day0 (D0) and day4 (D4) after intraluminal injection of distinct chloride concentrations ([Cl^-]): 5.8, 29, 143, and 715 mM Cl^-. **b**, **c** Morphometric analysis of **b** number of peripheral airway buds and **c** epithelial perimeter at the different [Cl^-]. Lower panel: **d** represents the fetal lung explants after intraluminal injection of distinct Cl^- channels inhibitors: anthracene-9-carboxylic acid (A9C) to transmembrane protein 16A TMEM16A; cystic fibrosis transmembrane conductance regulator inhibitor172 (CFTRinh) to CFTR; and calcium-dependent Cl^- channel inhibitorA01 (CaCCinh) to CaCC. **e**, **f** Morphometric analysis of **e** number of peripheral airway buds and **f** epithelial perimeter. Lungs were randomly assigned to one of eight experimental groups ($n \geq 12$ per condition). Results are expressed as the ratio of D4 and D0 (D4/D0) and presented as mean ± SD. Black rectangles define the control group. Scale bar, 1 mm. $p < {}^{\alpha}0.0001$, ${}^{\beta}0.001$, ${}^{\gamma}0.01$, ${}^{\mu}0.05$

PIEZO1 and PIEZO2 are expressed in pulmonary neuroendocrine cells during branching morphogenesis

To explore the molecular mechanism under branching morphogenesis and intraluminal composition, the spatial distribution of mechanosensors (PIEZO1 and PIEZO2) and neuroendocrine cell marker (PGP9.5) were determined in both in vivo and ex vivo branching morphogenesis. Immunofluorescence assay disclosed the colocalization of PIEZO1 (Fig. 2a) and PIEZO2 (Fig. 2b) with PGP9.5 at E17.5 and after intraluminal injection of SS or 143 mM Cl^- in ex vivo lung explant cultures (Fig. 2c-d). Concerning the [Cl^-] and Cl^- channels inhibitors, the similar expression profile observed for PIEZO1 (Fig. 2e) and PIEZO2 (Fig. 2f) in PGP9.5 + cells at 5.8 and 715 mM Cl^- contrast with the more restricted PIEZO1 (Fig. 2g) and PIEZO2 (Fig. 2h) pattern visualized in neuroendocrine cells after injection of CFTRinh or CaCCinh.

Intraluminal chloride concentration regulates ghrelin, bombesin, PIEZO1, and PIEZO2, expression levels

Since the PIEZO1 and PIEZO2 are expressed in neuroendocrine cells in branching morphogenesis, we then quantified by western blot the relative expression levels of receptors: PIEZO1, PIEZO2; and neuroendocrine products: ghrelin and bombesin, at the above-mentioned experimental conditions.

In comparison with 143 mM Cl^-, 715 mM was an inductor of ghrelin (Fig. 3a, b), bombesin (Fig. 3c), PIEZO1 (Fig. 3d), and PIEZO2 (Fig. 3e) expression, whereas 5.8 mM Cl^- inhibited the relative expression levels of ghrelin (Fig. 3a–e). Unchanged molecular profiles in terms of ghrelin (Fig. 3b), bombesin (Fig. 3c), PIEZO1 (Fig. 3d), or PIEZO2 (Fig. 3e) were detected analyzing 29 mM versus 143 mM Cl^-.

Regarding the Cl^- channels inhibition, distinct effects on ghrelin (Fig. 3f, g), bombesin (Fig. 3h), PIEZO1 (Fig. 3i), and PIEZO2 (Fig. 3j) expression were visualized after inhibition of TMEM16A by A9C, CFTR by CFTRinh, and CaCC by CaCCinh as demonstrated in Fig. 3f–j. Specifically, compared with SS, the injection of CFTRinh or CaCCinh were inhibitors of ghrelin (Fig. 3f, g), bombesin (Fig. 3h), PIEZO1 (Fig. 3i), and PIEZO2 (Fig. 3j) expression, whereas no significant modifications in the protein expression levels were observed after A9C injection (Fig. 3f–j).

PIEZO1 and PIEZO2 control branching morphogenesis

To evaluate the functional role of PIEZO1 and PIEZO2 in branching morphogenesis, the culture medium was supplemented with GsMTX4, a known pharmacological inhibitor of PIEZO1 and PIEZO2, on the day of intraluminal injections, D0 and D2.

The morphologic analysis showed a similar number of peripheral airway buds and epithelial perimeter after GsMTx4 medium supplementation and intraluminal injection of 5.8, 143, or 715 mM Cl^- (Fig. 4a–c). Indeed, the GsMTx4 inhibits branching morphogenesis at 143 and 715 mM Cl^-, whereas similar branching morphogenesis was observed at 5.8 mM Cl^- in normal and supplemented lungs. No significant differences in lung growth were detected between 5.8 mM Cl^- without GsMTx4 and 5.8, 143, or 715 mM with GsMTx4 (Fig. 4a–c). Concerning the Cl^- channels inhibition, the synchronous SS injection and PIEZO1/PIEZO2 downregulation triggered a relevant decrease in the number of peripheral airway buds (Fig. 4d, e). Oppositely, the decrease in branching morphogenesis induced by CFTR or CaCCs inhibitors (compared to SS normal) was unchanged by PIEZO1/PIEZO2 inhibition (Fig. 4d–f).

To better identify the PIEZO1/2 function in fetal lung growth, the relative expression levels of PIEZO1, PIEZO2, ghrelin, and bombesin were also evaluated at the abovementioned conditions. GsMTx4 treated-lung presented a decrease in PIEZO1 (Fig. 5a, b), PIEZO2 (Fig. 5c), bombesin (Fig. 5d), and ghrelin (Fig. 5e) expression at 143 and 715 mM Cl^- when compared with the GsMTx4 untreated-lungs (Fig. 5a–e). In contrast, PIEZO1 (Fig. 5a, b), PIEZO2 (Fig. 5c), bombesin (Fig. 5d), and ghrelin (Fig. 5e) expression levels remain unaffected comparing the injection of 5.8 mM Cl^- with and without GsMTx4.

Concerning the Cl^- channels inhibitors, we reported the GsMTx4 as an inhibitor of PIEZO1 (Fig. 5f, g), PIEZO2 (Fig. 5h), bombesin (Fig. 5i), and ghrelin (Fig. 5j) expression after intraluminal injection of SS. On the other hand, the simultaneous inhibition of PIEZO1/PIEZO2 and CFTR or CaCC injection had no additional effect on the relative expression levels of PIEZO1 (Fig. 5f, g), PIEZO2 (Fig. 5h), bombesin (Fig. 5i) or ghrelin (Fig. 5j).

The molecular effect of intraluminal injections in airway smooth muscle cells

Previous work reported a morphological interaction between branching morphogenesis and peristaltic airway contractions. Thus, we then assessed the molecular profile of MLC2 and α-SMA at the above-mentioned experimental conditions (Fig. 6a–c). Our findings revealed an opposite effect in the expression of MLC2 (Fig. 6b) and α-SMA (Fig. 6c) after injection of 5.8 or 715 mM Cl^-. Indeed, when compared with 143 mM Cl^-, 5.8 mM inhibits whereas 715 mM Cl^- promotes MLC2 (Fig. 6b) and α-SMA expression (Fig. 6c). Finally, the depletion

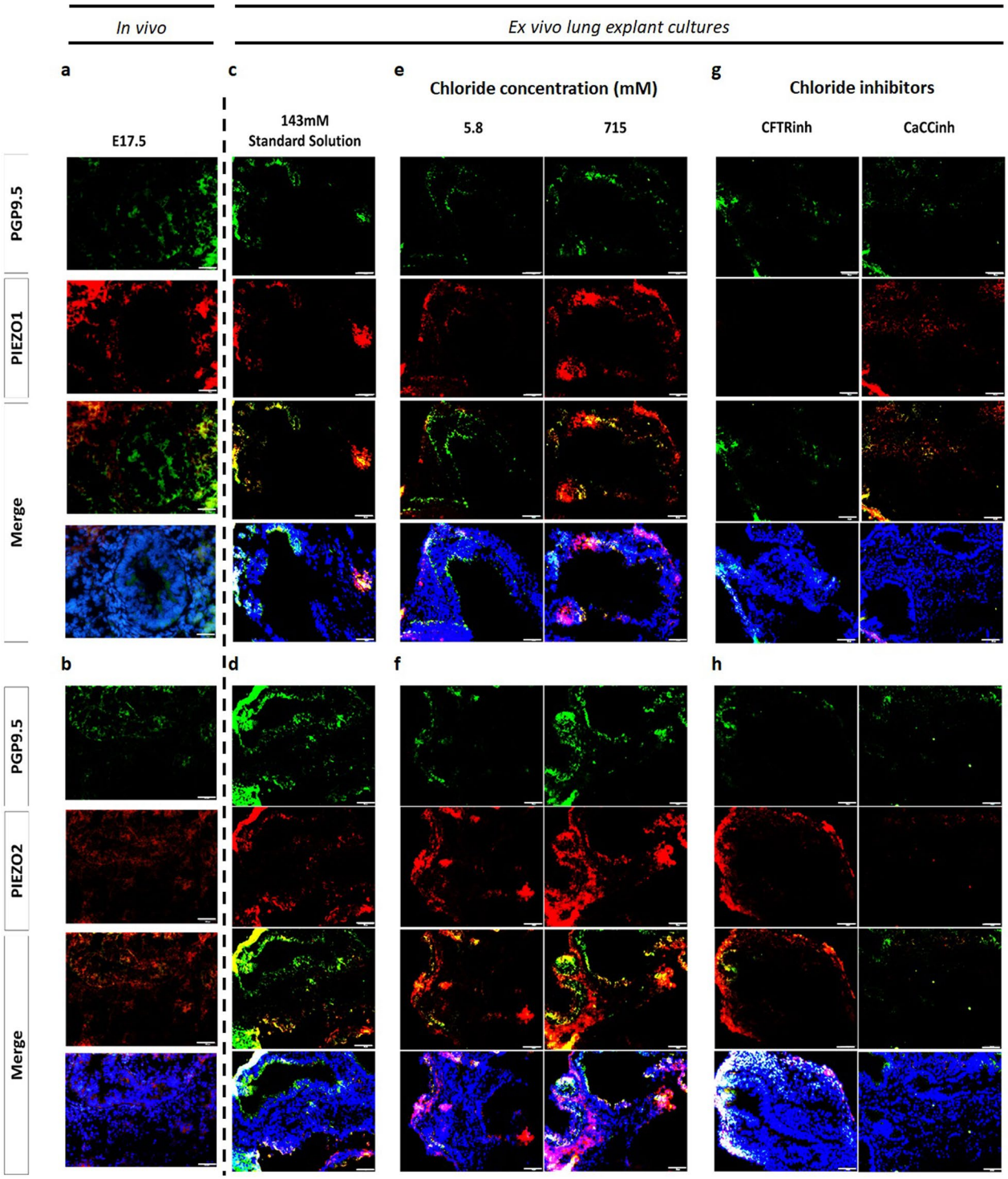

Fig. 2 Spatial distribution of PIEZO1 and PIEZO2 in in vivo and ex vivo branching morphogenesis. Representative examples of immunofluorescence assay for PIEZO1, PIEZO2, and PGP9.5 staining at **a**, **b** embryonic day (E)17.5; and after intraluminal injections of **c**, **d** 143 mM Cl^- or standard solution (SS); **e**, **f** different chloride concentrations ($[Cl^-]$): 5.8 and 715 mM Cl^-; and **g**, **h** Cl^- channel inhibitors: cystic fibrosis transmembrane conductance regulator inhibitor172 (CFTRinh) to CFTR; and calcium-dependent Cl^- channel inhibitor A01 (CaCCinh) to CaCCs. 143 mM Cl^- and standard solution (SS) represent the control condition for $[Cl^-]$ and Cl^- channels inhibitors, respectively, in which similar spatiotemporal distribution was observed. $n \geq 4$ per stage or condition/antibody for whole lungs and lung explants. Scale bar 50 µm

of PIEZO1/PIEZO2 expression achieved by GsMTx4 medium supplementation displayed a similar decrease in the relative expression levels of MLC2 (Fig. 6b) and α-SMA (Fig. 6c) at 143 and 715 mM Cl^- observed at D4. No differences in the relative expression levels were detected after injection of 5.8 mM Cl^- with and without GsMTx4.

Regarding the Cl^- channel inhibitors, after the intraluminal injection of CFTRinh or CaCCinh versus SS, a significant inhibitory effect was uncovered in MLC2 (Fig. 6d, e) and α-SMA (Fig. 6f). In addition, GsMTx4 medium supplementation only decreased the relative expression levels of MLC2 (Fig. 6e) and α-SMA (Fig. 6f) previously observed after SS intraluminal. No additional effect in MLC2 (Fig. 6e) or α-SMA (Fig. 6f) were visualized after simultaneously GsMTX4 medium supplementation and intraluminal injections of CFTRinh or CaCCinh (Fig. 6d–f).

Discussion

The fetal lung develops as a fluid-filled organ that maintains the lung in a constantly distended state, stimulating its growth and maturation [60–63]. Unfortunately, the difficulty of capturing or recapitulating the in vivo morphological dynamics in the lab hinders the study of the underlying mechanisms, particularly at early developmental stages. In this context, ex vivo lung explant cultures are an asset since it maintains the in vivo physiologic architecture and the cellular interactions observed at the pseudoglandular or branching stage [57, 64]. Bearing this in mind, we established effective intraluminal injections at D0 and D2 and observed dynamic movements in the lumen at D4, indicating the existence of lung liquid in the ex vivo model and validating this approach as a valuable method for studying lung fluid composition in branching morphogenesis.

On the strongly evidenced premise that the Cl^- movement in the epithelium is an inductor of Na^+ and water movements in the same direction [22–25, 65–67], we manipulated the intraluminal lung fluid composition by injecting different [Cl^-] or Cl^- channel inhibitors and then analyzing the branching morphogenesis at D4. Our findings demonstrated that intraluminal [Cl^-] was able to regulate fetal lung growth. In fact, the increase of luminal [Cl^-] stimulated branching morphogenesis, whereas a significant decrease was observed after depletion of [Cl^-] at 5.8 mM Cl^- (Fig. 7). No significant effect was identified in branching morphogenesis at 29 mM Cl^-. These results further indicate distinct capacities for the injected solutions to imbalance the extracellular versus intracellular ionic charges, as previously predicted by mathematical models. For instance, the Gibbs-Donnan effect establishes that charged particles near a semi-permeable membrane sometimes fail to distribute evenly across the two sides of the membrane. In addition, the potential equilibrium for Cl^- calculated from the Nernst equation [68] supports our knowledge regarding the differences between the intracellular versus extracellular manipulation of [Cl^-]. Both effects were demonstrated in neuronal membranes and point to features governing fluid exchange between the intra and extracellular environment of cells [69, 70]. In our model, the manipulation of extracellular [Cl^-] suggests a range, higher than 29 mM Cl^-, compatible with normal fetal lung development, indicating an interesting effect for the in vivo lung fluid production and maintenance of a suitable environment for lung cells. Curiously, experiments in fetal sheep have demonstrated a direct link between reduced distension due to fluid loss and lung hypoplasia. Conversely, tracheal obstruction in utero leads to fluid accumulation and more rapid lung growth [71]. These differences in pressure between the airway lumen and surrounding tissue are essential for normal airway development, with tension and mechanical stretch playing additional roles in cellular differentiation and airway growth [72].

Regarding the Cl^- channel inhibitors, fluid secretion into the airway lumen is driven by Cl^- transport, which is mediated by at least two types of anion channels, CaCC and CFTR, that respond to different stimuli: intracellular Ca^{2+} and cAMP, respectively [73–75]. Conversely, an interdependent function for CFTR and TMEM16A has been demonstrated in adult mice and human respiratory and intestinal epithelial cells [76]. Our study suggests a comparable strong effect of both CFTR and CaCC in lung fluid production and branching morphogenesis. In contrast, the reported unchanged branching morphogenesis after A9C injection, an inhibitor of TMEM16A [77], indicates an insufficient or quickly compensated

(See figure on next page.)

Fig. 3 Intraluminal chloride modulates the expression of ghrelin, bombesin, PIEZO1, and PIEZO2. **a**–**e** Upper panel represents the main effects of the distinct chloride concentrations ([Cl^-]). **a** Examples of representative blots are shown. **b**–**e** Relative expression levels of **b** ghrelin, **c** bombesin, **d** PIEZO1, and **e** PIEZO2. **f**–**j** Lower panel shows the molecular effect of intraluminal Cl^- channels inhibition by anthracene-9-carboxylic acid (A9C) to transmembrane protein 16A (TMEM16A); cystic fibrosis transmembrane conductance regulator inhibitor172 (CFTRinh) to CFTR and calcium-dependent Cl^- channel inhibitor A01 (CaCCinh) to CaCCs. **f** Examples of representative blots are shown. **g**–**j** Protein expression levels for **g** ghrelin, **h** bombesin, **i** PIEZO1 and **j** PIEZO2. Black rectangles define the control group. Each lane represents a pooled-tissue sample, and relative expression levels were determined against GAPDH. $n \geq 4$ were used per antibody/condition. Results are presented as mean ± SD. Symbols indicate the main effects and non-redundant interactions of the one-way ANOVA. $p < {}^{\alpha}0.0001$

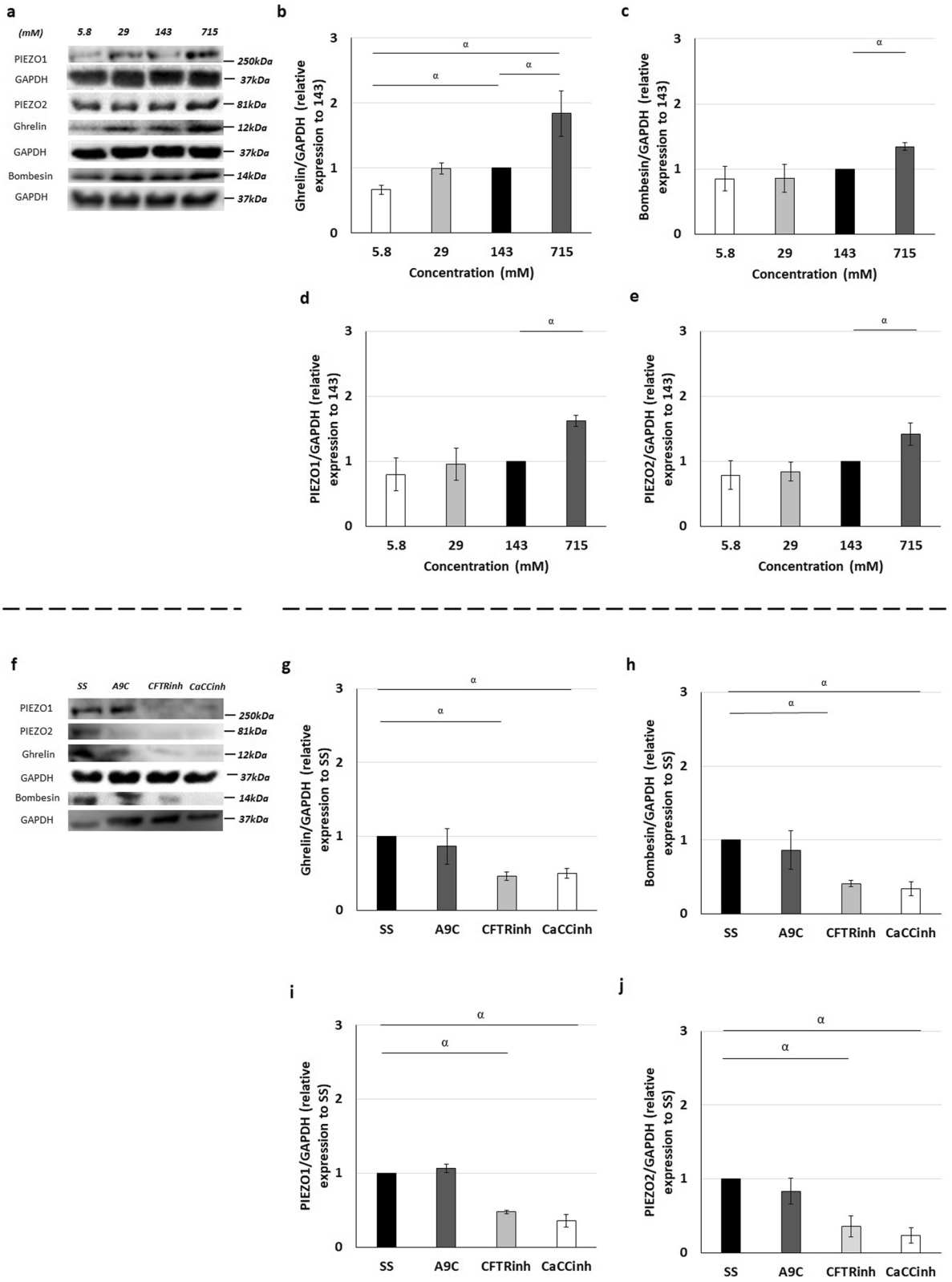

Fig. 3 (See legend on previous page.)

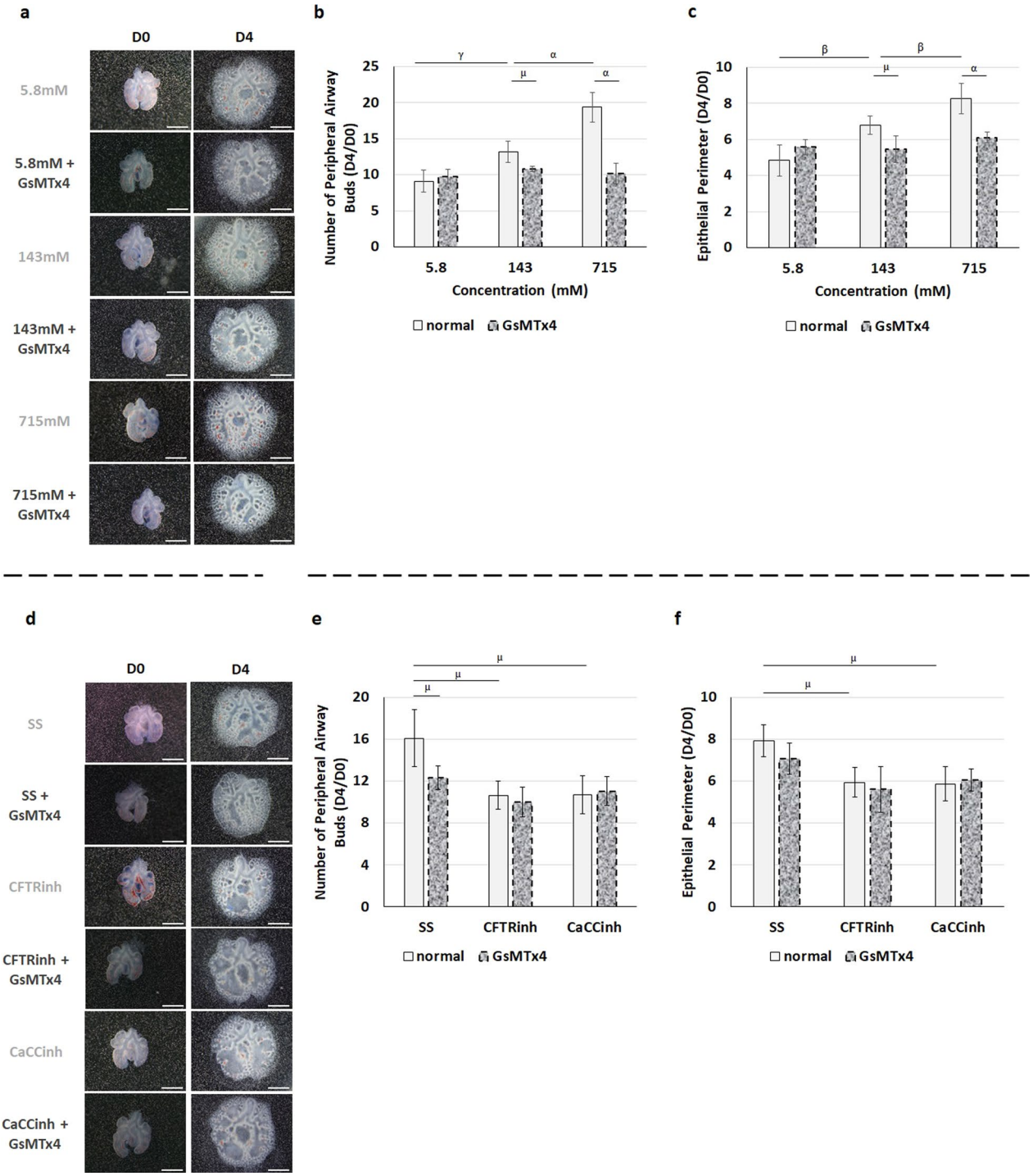

Fig. 4 PIEZO1 and PIEZO2 mediate the effects of manipulating intraluminal chloride. **a**–**c** Upper panel represents the main cumulative effect of intraluminal injection of distinct chloride concentrations ($[Cl^-]$) 5.8, 143, or 715 mM Cl^- and the medium supplementation with GsMTx4 at day0 (D0) and day2 (D2). **a** Represents lung explants at D0 and D4 for the different $[Cl^-]$. **b**, **c** Morphometric analysis of **b** peripheral airway buds and **c** epithelial perimeter. **d**–**f** Lower panel shows the additional effect of PIEZO1/2 inhibition after intraluminal injection of Cl^- channels inhibitors: cystic fibrosis transmembrane conductance regulator inhibitor172 (CFTRinh) to CFTR; and calcium-dependent Cl^- channel inhibitor A01 (CaCCinh) to CaCCs. **d** represents the fetal lung explants at D0 and D4 for the distinct Cl^- channels inhibitors. **e**, **f** Morphometric analysis of **e** peripheral airway buds and **f** epithelial perimeter. 143 mM Cl^- and standard solution (SS) identified the control condition for $[Cl^-]$ and Cl^- channels inhibitors, respectively. White and dotted rectangles represent the medium supplementation with and without GsMTx4, respectively. $n \geq 4$ were used per antibody/condition. Results are expressed as the ratio of D4 and D0 (D4/D0) and presented as mean ± SD. Symbols indicate the main effects and non-redundant interactions of the two-way ANOVA. $p < {}^{\alpha}0.0001$, ${}^{\beta}0.001$, ${}^{\gamma}0.01$, ${}^{\mu}0.05$

function for TMEM16A in lung fluid secretion. Brennan et al. [20] also described TMEM16A and bestrophin1 as insufficient for Ca^{2+}-stimulated lung fluid secretion in the mouse fetal lung. Finally, the molecular inhibition of ionic channels, such as CFTR, ClC2, or CaR, critical for lung fluid secretion, induces key defects in vivo and ex vivo branching morphogenesis [18, 20, 21, 26, 27, 30, 78] that reinforce the value of our ex vivo model for the study of intraluminal fluid in fetal lung growth.

Collectively, these findings prompt us to go further in the inherent molecular/cellular mechanisms. As such, our data demonstrated that PIEZO1 and PIEZO2 colocalize with PGP9.5, a molecular marker for PNECs/NEBs. Interestingly, PIEZO1 and PIEZO2 receptors are sensors for mechanical stretch, like pressure, with major roles in regulating blood pressure and respiratory function at birth, respectively [41, 45, 79]. In contrast, PNECs/NEBs are described as airway sensors with poorly understood functions [40]. Literature also shows that the secreted neuroendocrine products, ghrelin, and bombesin, are promotors of the in vivo and ex vivo fetal lung growth [35–39]. To further investigate these dynamics, neuroendocrine products (ghrelin, bombesin) and mechanoreceptors (PIEZO1 and PIEZO2) were quantified at the abovementioned conditions. We found that the intraluminal [Cl^-] modulates ghrelin, bombesin, PIEZO1, and PIEZO2 expression in branching morphogenesis. Briefly, the decrease of luminal [Cl^-], 5.8 mM Cl^-, was an inhibitor of ghrelin with no significant effects on the expression of the remaining markers (Fig. 7). Surprisingly, 715 mM Cl^- stimulated ghrelin, bombesin, PIEZO1, and PIEZO2 expression, whereas the luminal injection of CFTRinh or CaCCinh inhibited fetal lung growth and equally inhibited the four markers (Fig. 7).

Dickson et al. [9] described the lung liquid as a regulator of fetal lung growth in a mechanism independent of the lung fluid secretion and suggested that the lung is unable to respond to alterations in lung liquid volume. Indeed, the decrease in pulmonary growth was related to reduced tracheal pressure and tracheal efflux rate in the fetal sheep model. Now, our analysis revealed that PIEZO1, PIEZO2, and bombesin were overexpressed at 715 mM Cl^- and unchanged at 5.8 mM Cl^-, when compared with the basal [Cl^-], 143 mM. As such, it is important to define the fundamental responses in fetal lung growth after PIEZO1/PIEZO2 inhibition. For that, we inhibited the PIEZO1/PIEZO2 on the day of intraluminal injections by GsMTx4. We demonstrated a significant inhibition of neuroendocrine products and branching morphogenesis after GsMTx4 medium supplementation. More importantly, this outcome was independent of the intraluminal [Cl^-]. In fact, apart from 5.8 mM Cl^- where no significant differences between GsMTx4-treated and -untreated lungs were observed, the intraluminal injection of 143, 715 mM Cl^- or SS with the synchronized inhibition of PIEZO1/PIEZO2 by GsMTx4 similarly decreased the morphological and molecular profiles. These findings indicate that PIEZO1 and PIEZO2 are major regulators of the mechanosensory pathway in branching morphogenesis. A recent publication showed PIEZO2 as a regulator of pulmonary function in neonates and adults [41]. Indeed, the global and sensory neuron-specific ablation of mechanically activated ion channel PIEZO2 causes respiratory distress and death in newborn mice. In contrast, the induced ablation of PIEZO2 in sensory neurons of adult mice causes decreased neuronal responses to lung inflation and an impaired Hering-Breuer mechanoreflex [41]. In this context, our investigation suggests that PIEZO1/PIEZO2, present in PNECs/NEBs, act as sensors of branching morphogenesis in fetal lung development.

Physiology has shown that the movement of intraluminal fluid through epithelial tubules is a consequence of the peristaltic activity of fetal airway smooth muscle (ASM) that maintains positive pressure in the lumen area to keep the tubules in a distended state [62]. The formation of new airspaces during branching morphogenesis early in gestation is closely followed by the differentiation of mesenchymal cells into ASM cells. Evidenced by cellular expression of the contractile protein α-SMA as an early differentiation marker [80], ASM progenitor cells have been identified in both the proximal and distal lung mesenchyme [81, 82]. This differentiation of ASM simultaneously produces the MLC filaments in fetal lungs [31–34, 83–85]. To determine the molecular effect of intraluminal Cl^- composition in airway smooth muscle cells, we evaluated α-SMA and MLC2 at the aforementioned experimental condition with and without

(See figure on next page.)

Fig. 5 Decrease of PIEZO1 and PIEZO2 expression removes the molecular dynamics triggered by intraluminal chloride concentration. **a**–**e** Upper panel represents the main cumulative effect of intraluminal chloride concentration ([Cl^-]) and medium supplementation with (dotted rectangles) and without (white rectangles) GsMTx4. **a** Examples of representative blots are shown. **b**–**e** Protein expression levels for **b** PIEZO1, **c** PIEZO2, **d** bombesin, and **e** ghrelin are indicated. **f**–**j** Lower panel shows the additional effect of GsMTx4 after intraluminal injection of Cl^- channels inhibitors: cystic fibrosis transmembrane conductance regulator inhibitor172 (CFTRinh) to CFTR; and calcium-dependent Cl^- channel inhibitor A01 (CaCCinh) to CaCCs. **f** Examples of representative blots are shown. **g**–**j** Relative expression levels of **g** PIEZO1, **h** PIEZO2, **i** bombesin, and **j** ghrelin. 143 mM Cl^- and standard solution (SS) represent the control condition for [Cl^-] and Cl^- channels inhibitors, respectively. $n \geq 4$ were used per antibody/condition. Results are presented as mean ± SD. Symbols indicate the main effects and non-redundant interactions of the two-way ANOVA. $p < {}^{\alpha}0.0001$

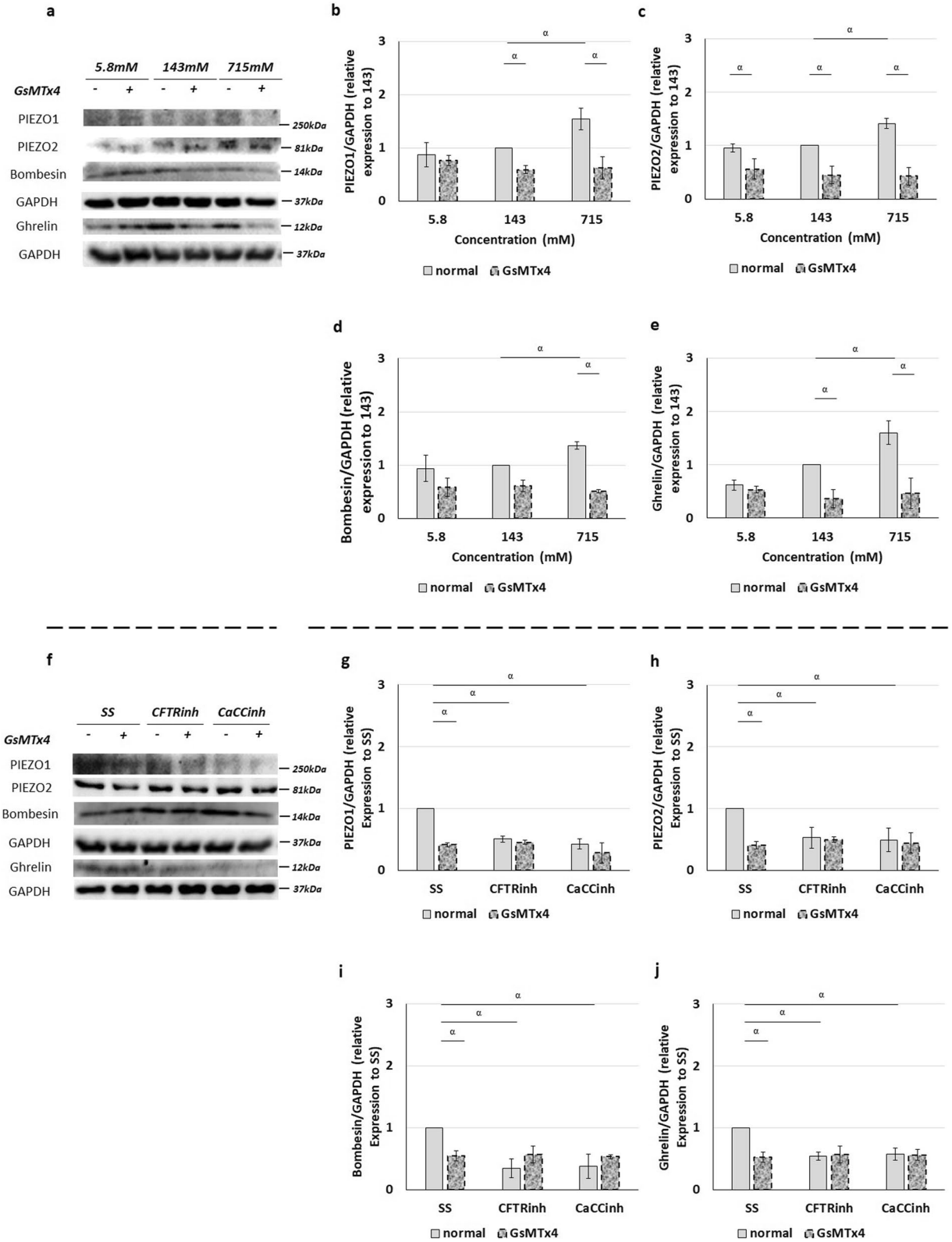

Fig. 5 (See legend on previous page.)

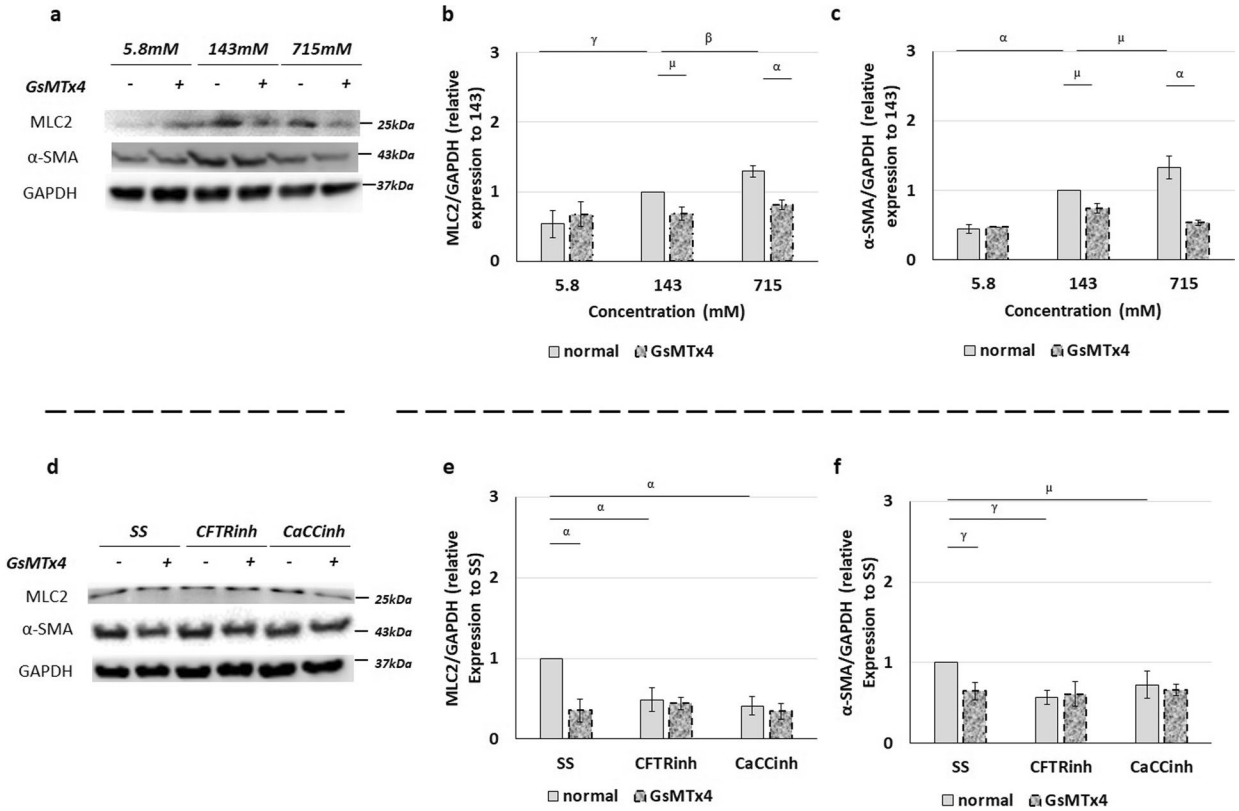

Fig. 6 Molecular effect of intraluminal chloride and GsMTx4 in smooth muscle cells. **a-c** Upper panel represents the main cumulative effect of intraluminal chloride concentration ($[Cl^-]$) and medium supplementation with and without GsMTx4. **a** Examples of representative blots are shown. **b**, **c** Protein expression levels for **b** myosin light chain 2 (MLC2), and **c** alpha-smooth muscle actin (α-SMA) are quantified. **d–f** Lower panel shows the additional effect of PIEZO1/2 inhibition after intraluminal injection of Cl^- channels inhibitors: cystic fibrosis transmembrane conductance regulator inhibitor172 (CFTRinh) to CFTR and; calcium-dependent Cl^- channel inhibitor A01 (CaCCinh) to CaCCs. **d** Examples of representative blots are shown. **e–f** Relative expression levels of **e** MLC2, and **f** α-SMA are displayed. 143 mM Cl^- and standard solution (SS) represent the control condition for $[Cl^-]$ and Cl^- channels inhibitors, respectively. White and dotted rectangles represent the medium supplementation with and without GsMTx4, respectively. Each lane represents a pooled-tissue sample, and the relative expression levels were determined against GAPDH. $n \geq 4$ were used per antibody/condition. Results are presented as mean ± SD. Symbols indicate the main effects and non-redundant interactions of the two-way ANOVA. $p < {}^{\alpha}0.0001$, ${}^{\beta}0.001$, ${}^{\gamma}0.01$, ${}^{\mu}0.05$

GsMTx4. We observed that the increase of $[Cl^-]$ and branching morphogenesis relates to the overexpression of MLC2 and α-SMA. Conversely, the decrease in α-SMA and MLC2 were associated with reduced $[Cl^-]$ and branching morphogenesis (Fig. 7). One can argue that the increase/decrease in ASM markers may either alter the frequency or the force of peristaltic airway contractions thus altering peristalsis effect on lung growth [86].

Overall, these results indicated that the intraluminal composition and the neuroendocrine activation act upstream of airway smooth muscle contraction and branching morphogenesis. Interestingly, the hypoplastic phenotype observed in the CDH context was connected to a decrease in α-SMA and MLC2 from the pseudoglandular-to-canalicular stage [32]. In contrast, tracheal occlusion in in vivo mouse model was an inductor of α-SMA and MLC2 expression at the later canalicular stage [87], suggesting that the PIEZO1/PIEZO2 pathway may be a potential target for the treatment of fetal pulmonary hypoplasia.

Conclusions

Our findings offer a mechanistic basis for previous in vivo data that reported an excess of fluid drainage during fetal life or a decreased fluid pressure associated with lung hypoplasia with underbranched lungs. Here, we describe key information on the specific pathway by which the intraluminal Cl^- composition regulates fetal lung growth. We demonstrate that the intraluminal $[Cl^-]$ activates PNECs/NEBs through PIEZO1/PIEZO2 mechanoreceptors that, in turn, regulate the expression of ghrelin, bombesin, α-SMA, and MLC2 thus regulating fetal lung growth (Fig. 7).

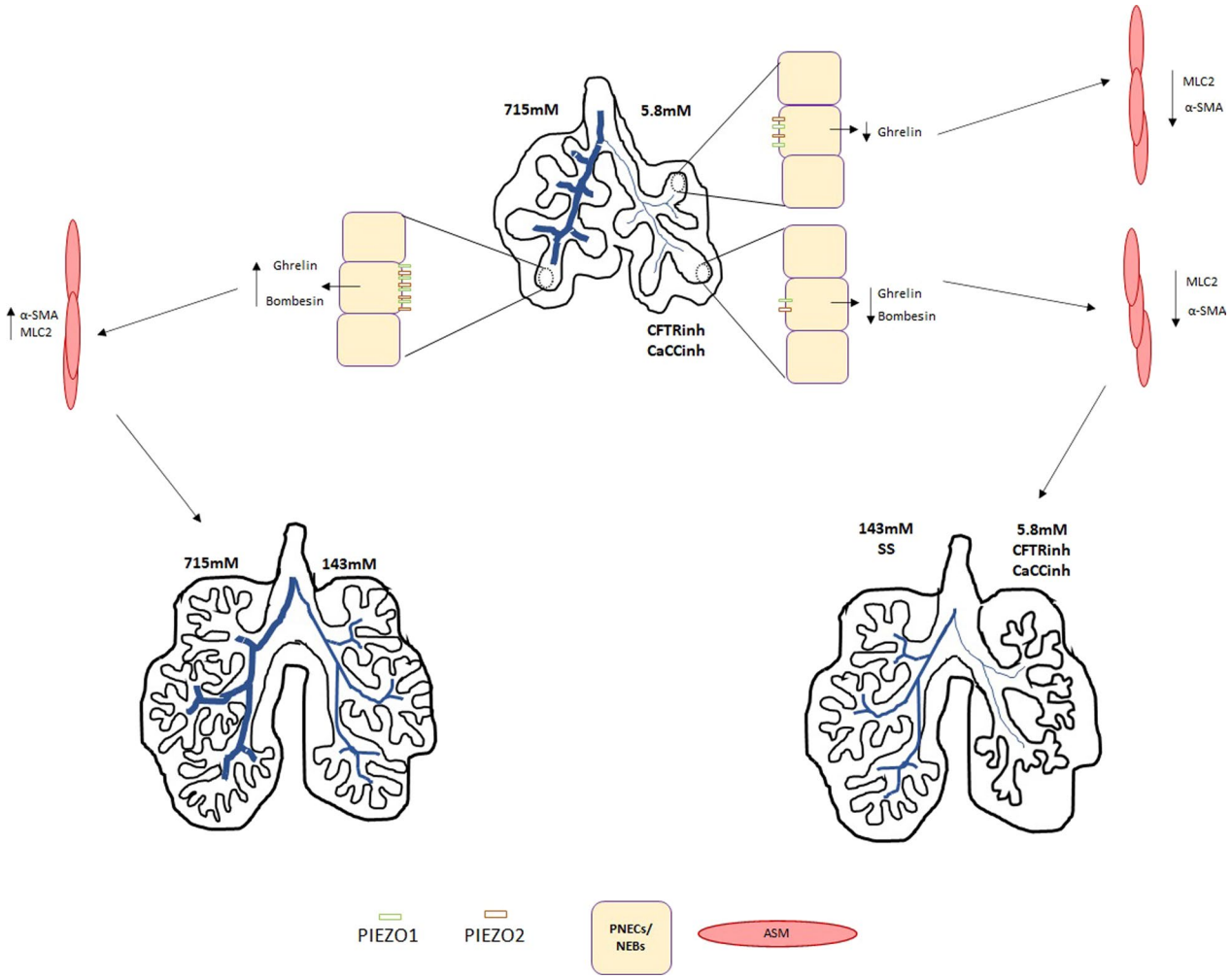

Fig. 7 Schematic representation of the role of intraluminal chloride concentrations in fetal branching morphogenesis. Increasing concentrations of intraluminal [Cl^-] leads to increased branching morphogenesis and expression of neuroendocrine products, PIEZO channels, and smooth muscle markers. Pharmacological inhibition experiments show that these effects require PIEZO and Cl^- channel activation. α-SMA, alpha-smooth muscle actin; CaCCinh calcium-dependent Cl^- channel inhibitorA01; CFTRinh, cystic fibrosis transmembrane conductance regulator inhibitor172; MLC2, myosin light chain 2; SS, standard solution

Abbreviations

[Cl^-]	Chloride concentration
A9C	Anthracene-9-carboxylic acid
BSA	Bovine serum albumin
Ca^{2+}	Calcium
CaCC	Calcium-dependent chloride channel
CaCCinh	Calcium-dependent chloride inhibitorA01
$CaCl_2$	Calcium chloride
CaR	Calcium receptor
CDH	Congenital diaphragmatic hernia
CFTR	Cystic fibrosis transmembrane conductance regulator
CFTRinh	Cystic fibrosis transmembrane conductance regulator inhibitor172
Cl^-	Chloride
ClC_2	Chloride channel2
CO_2	Carbon dioxide
D0	Day 0;
DAPI	4′,6-Diamidino-2-phenylindole
DMEM	Dulbecco's Modified Eagle Medium
DMSO	Dimethyl sulfoxide
E	Embryonic day
FBS	Fetal bovine serum
FETO	Fetoscopic endoluminal tracheal occlusion
GAPDH	Glyceraldehyde-3-phosphate dehydrogenase
HEPES	4-(2-Hydroxyethyl)-1-piperazineethanesulfonic acid
K^+	Potassium
KCl	Potassium chloride
Mg^{2+}	Magnesium
$MgCl_2$	Magnesium chloride
$MgSO_4$	Magnesium sulfate
MLC_2	Myosin light chain 2
Na/K/2Cl	Sodium–potassium-2chloride cotransporter
Na/K-ATPase	Sodium–potassium adenosine triphosphatase pump
NaCl	Sodium chloride
NEBs	Neuroepithelial bodies
PBS	Phosphate buffered saline
PGP9.5	Protein gene product 9.5
PNECs	Pulmonary neuroendocrine cells

RT	Room temperature
SS	Standard solution
TMEM16A	Transmembrane protein 16A
α-SMA	Alpha-smooth muscle actin

Supplementary Information

The online version contains supplementary material available at https://doi.org/10.1186/s12931-023-02328-2.

Additional file 1: Table S1. Summary of chemical compounds in injected solution used for manipulation of the intraluminal fluid. **a** show the chemical concentration by compound for standard solution (SS) and crescent chloride concentrations, [Cl^-]: 5.8, 29, 143, and 715 mM. **b** demonstrates the ionic composition in terms of chloride (Cl^-), potassium (K^+), magnesium (Mg^{2+}) and calcium (Ca^{2+}) in SS, 5.8, 29, 143 and 715 mM Cl^-.

Additional file 2: Movie S1. Injection of standard solution into the lumen of ex vivo lung explant cultures at day0 (D0).

Additional file 3: Movie S2. Injection of standard solution into the lumen of ex vivo lung explant cultures at day2 (D2).

Additional file 4: Movie S3. Dynamic intraluminal movement in ex vivo lung explant cultures at day4 (D4).

Acknowledgements
We are indebted to Goreti Pinto, Magda Carlos and Alice Miranda for expert technical assistance.

Author contributions
ANG performed the research and wrote the paper; ANG and CNS designed the research; ANG, CNS and JCP analyzed and interpreted the data; RSM revised and edited the manuscript and reanalyzed results. All authors read and approved the final version of the manuscript.

Funding
This work has been funded by National funds, through the Foundation for Science and Technology (FCT)—project UIDB/50026/2020; by the projects NORTE-01-0145-FEDER-000013 and NORTE-01-0145-FEDER-000023, supported by Norte Portugal Regional Operational Programme (NORTE 2020), under the PORTUGAL 2020 Partnership Agreement, through the European Regional Development Fund (ERDF); and by ICVS Scientific Microscopy Platform, member of the national infrastructure PPBI—Portuguese Platform of Bioimaging (PPBI-POCI-01-0145-FEDER-022122); This work was also funded by POCI-01-0145-FEDER-030881, financed by Fundos Europeus Estruturais e de Investimento (FEEI) and FCT. ANG was supported by FCT and the company José de Mello Saúde S.A.—2CA Braga (reference PD/BDE/127829/2016). The funders had no role in study design, data collection, and analysis, decision to publish, or preparation of the manuscript.

Availability of data and materials
The authors declare that the data supporting the findings of the present study are available within the manuscript or from the corresponding author upon reasonable request.

Declarations

Ethics approval and consent to participate
This study was carried out in strict accordance with FELASA guidelines [88] and European regulations (European Union Directive 86/609/EEC). All animal experiments were approved by the Life and Health Sciences Research Institute (ICVS), University of Minho, and by the Direção Geral de Alimentação e Veterinária (approval No. DGAV 021328).

Consent for publication
Not applicable.

Competing interests
The authors declare that they have no competing interest.

Received: 30 April 2022 Accepted: 13 January 2023
Published online: 05 February 2023

References

1. Moessinger AC, Collins MH, Blanc WA, Rey HR, James LS. Oligohydramnios-induced lung hypoplasia: the influence of timing and duration in gestation. Pediatr Res. 1986;20:951–4.
2. Harding R, Hooper SB, Dickson KA. A mechanism leading to reduced lung expansion and lung hypoplasia in fetal sheep during oligohydramnios. Am J Obstet Gynecol. 1990;163:1904–13.
3. Copland I, Post M. Lung development and fetal lung growth. Paediatr Respir Rev. 2004;5(Suppl A):S259-264.
4. Shi W, Bellusci S, Warburton D. Lung development and adult lung diseases. Chest. 2007;132:651–6.
5. Wilson SM, Olver RE, Walters DV. Developmental regulation of lumenal lung fluid and electrolyte transport. Respir Physiol Neurobiol. 2007;159:247–55.
6. Jani JC, Nicolaides KH. Fetal surgery for severe congenital diaphragmatic hernia? Ultrasound Obstet Gynecol. 2012;39:7–9.
7. Jani JC, Benachi A, Nicolaides KH, Allegaert K, Gratacós E, Mazkereth R, Matis J, Tibboel D, Van Heijst A, Storme L, et al. Prenatal prediction of neonatal morbidity in survivors with congenital diaphragmatic hernia: a multicenter study. Ultrasound Obstet Gynecol. 2009;33:64–9.
8. Gonçalves AN, Correia-Pinto J, Nogueira-Silva C. Imagiological methods for prediction of fetal pulmonary hypoplasia: a systematic review. J Matern Fetal Neonatal Med. 2021;34:1459–68.
9. Dickson KA, Harding R. Restoration of lung liquid volume following its acute alteration in fetal sheep. J Physiol. 1987;385:531–43.
10. Fletcher AJ, Edwards CM, Gardner DS, Fowden AL, Giussani DA. Neuropeptide Y in the sheep fetus: effects of acute hypoxemia and dexamethasone during late gestation. Endocrinology. 2000;141:3976–82.
11. Khan PA, Cloutier M, Piedboeuf B. Tracheal occlusion: a review of obstructing fetal lungs to make them grow and mature. Am J Med Genet C Semin Med Genet. 2007;145:125–38.
12. Unbekandt M, del Moral PM, Sala FG, Bellusci S, Warburton D, Fleury V. Tracheal occlusion increases the rate of epithelial branching of embryonic mouse lung via the FGF10-FGFR2b-Sprouty2 pathway. Mech Dev. 2008;125:314–24.
13. Jiménez JA, Eixarch E, DeKoninck P, Bennini JR, Devlieger R, Peralta CF, Gratacos E, Deprest J. Balloon removal after fetoscopic endoluminal tracheal occlusion for congenital diaphragmatic hernia. Am J Obstet Gynecol. 2017;217:78.e71-78.e11.
14. Ruano R, Peiro JL, da Silva MM, Campos JA, Carreras E, Tannuri U, Zugaib M. Early fetoscopic tracheal occlusion for extremely severe pulmonary hypoplasia in isolated congenital diaphragmatic hernia: preliminary results. Ultrasound Obstet Gynecol. 2013;42:70–6.
15. Ali K, Bendapudi P, Polubothu S, Andradi G, Ofuya M, Peacock J, Hickey A, Davenport M, Nicolaides K, Greenough A. Congenital diaphragmatic hernia-influence of fetoscopic tracheal occlusion on outcomes and predictors of survival. Eur J Pediatr. 2016;175:1071–6.
16. Khoshgoo N, Kholdebarin R, Pereira-Terra P, Mahood TH, Falk L, Day CA, Iwasiow BM, Zhu F, Mulhall D, Fraser C, et al. Prenatal microRNA miR-200b therapy improves nitrofen-induced pulmonary hypoplasia associated with congenital diaphragmatic hernia. Ann Surg. 2019;269:979–87.
17. Gillie DJ, Pace AJ, Coakley RJ, Koller BH, Barker PM. Liquid and ion transport by fetal airway and lung epithelia of mice deficient in sodium-potassium-2-chloride transporter. Am J Respir Cell Mol Biol. 2001;25:14–20.
18. Finney BA, del Moral PM, Wilkinson WJ, Cayzac S, Cole M, Warburton D, Kemp PJ, Riccardi D. Regulation of mouse lung development by the extracellular calcium-sensing receptor. CaR J Physiol. 2008;586:6007–19.
19. Bardou O, Trinh NT, Brochiero E. Molecular diversity and function of K^+ channels in airway and alveolar epithelial cells. Am J Physiol Lung Cell Mol Physiol. 2009;296:L145-155.
20. Brennan SC, Wilkinson WJ, Tseng HE, Finney B, Monk B, Dibble H, Quilliam S, Warburton D, Galietta LJ, Kemp PJ, Riccardi D. The extracellular calcium-sensing receptor regulates human fetal lung development via CFTR. Sci Rep. 2016;6:21975.

21. Brennan SC, Finney BA, Lazarou M, Rosser AE, Scherf C, Adriaensen D, Kemp PJ, Riccardi D. Fetal calcium regulates branching morphogenesis in the developing human and mouse lung: involvement of voltage-gated calcium channels. PLoS ONE. 2013;8: e80294.
22. Olver RE, Strang LB. Ion fluxes across the pulmonary epithelium and the secretion of lung liquid in the foetal lamb. J Physiol. 1974;241:327–57.
23. Olver RE, Schneeberger EE, Walters DV. Epithelial solute permeability, ion transport and tight junction morphology in the developing lung of the fetal lamb. J Physiol. 1981;315:395–412.
24. Welsh MJ, Smith PL, Frizzell RA. Chloride secretion by canine tracheal epithelium: II. The cellular electrical potential profile. J Membr Biol. 1982;70:227–38.
25. Welsh MJ. Evidence for basolateral membrane potassium conductance in canine tracheal epithelium. Am J Physiol. 1983;244:C377-384.
26. Blaisdell CJ, Morales MM, Andrade AC, Bamford P, Wasicko M, Welling P. Inhibition of CLC-2 chloride channel expression interrupts expansion of fetal lung cysts. Am J Physiol Lung Cell Mol Physiol. 2004;286:L420-426.
27. Larson JE, Cohen JC. Improvement of pulmonary hypoplasia associated with congenital diaphragmatic hernia by in utero CFTR gene therapy. Am J Physiol Lung Cell Mol Physiol. 2006;291:L4-10.
28. Ousingsawat J, Martins JR, Schreiber R, Rock JR, Harfe BD, Kunzelmann K. Loss of TMEM16A causes a defect in epithelial Ca^{2+}-dependent chloride transport. J Biol Chem. 2009;284:28698–703.
29. Rock JR, Onaitis MW, Rawlins EL, Lu Y, Clark CP, Xue Y, Randell SH, Hogan BL. Basal cells as stem cells of the mouse trachea and human airway epithelium. Proc Natl Acad Sci USA. 2009;106:12771–5.
30. Meyerholz DK, Stoltz DA, Gansemer ND, Ernst SE, Cook DP, Strub MD, LeClair EN, Barker CK, Adam RJ, Leidinger MR, et al. Lack of cystic fibrosis transmembrane conductance regulator disrupts fetal airway development in pigs. Lab Invest. 2018;98:825–38.
31. Schittny JC, Miserocchi G, Sparrow MP. Spontaneous peristaltic airway contractions propel lung liquid through the bronchial tree of intact and fetal lung explants. Am J Respir Cell Mol Biol. 2000;23:11–8.
32. Santos M, Moura RS, Gonzaga S, Nogueira-Silva C, Ohlmeier S, Correia-Pinto J. Embryonic essential myosin light chain regulates fetal lung development in rats. Am J Respir Cell Mol Biol. 2007;37:330–8.
33. Kim HY, Pang MF, Varner VD, Kojima L, Miller E, Radisky DC, Nelson CM. Localized smooth muscle differentiation is essential for epithelial bifurcation during branching morphogenesis of the mammalian lung. Dev Cell. 2015;34:719–26.
34. Goodwin K, Mao S, Guyomar T, Miller E, Radisky DC, Košmrlj A, Nelson CM. Smooth muscle differentiation shapes domain branches during mouse lung development. Development. 2019; 146.
35. Sunday ME, Hua J, Dai HB, Nusrat A, Torday JS. Bombesin increases fetal lung growth and maturation in utero and in organ culture. Am J Respir Cell Mol Biol. 1990;3:199–205.
36. Santos M, Bastos P, Gonzaga S, Roriz JM, Baptista MJ, Nogueira-Silva C, Melo-Rocha G, Henriques-Coelho T, Roncon-Albuquerque R Jr, Leite-Moreira AF, et al. Ghrelin expression in human and rat fetal lungs and the effect of ghrelin administration in nitrofen-induced congenital diaphragmatic hernia. Pediatr Res. 2006;59:531–7.
37. Nunes S, Nogueira-Silva C, Dias E, Moura RS, Correia-Pinto J. Ghrelin and obestatin: different role in fetal lung development? Peptides. 2008;29:2150–8.
38. Sakai K, Kimura O, Furukawa T, Fumino S, Higuchi K, Wakao J, Kimura K, Aoi S, Masumoto K, Tajiri T. Prenatal administration of neuropeptide bombesin promotes lung development in a rat model of nitrofen-induced congenital diaphragmatic hernia. J Pediatr Surg. 2014;49:1749–52.
39. Pereira-Terra P, Moura RS, Nogueira-Silva C, Correia-Pinto J. Neuroendocrine factors regulate retinoic acid receptors in normal and hypoplastic lung development. J Physiol. 2015;593:3301–11.
40. Garg A, Sui P, Verheyden JM, Young LR, Sun X. Consider the lung as a sensory organ: a tip from pulmonary neuroendocrine cells. Curr Top Dev Biol. 2019;132:67–89.
41. Nonomura K, Woo SH, Chang RB, Gillich A, Qiu Z, Francisco AG, Ranade SS, Liberles SD, Patapoutian A. Piezo2 senses airway stretch and mediates lung inflation-induced apnoea. Nature. 2017;541:176–81.
42. Wang F, Knutson K, Alcaino C, Linden DR, Gibbons SJ, Kashyap P, Grover M, Oeckler R, Gottlieb PA, Li HJ, et al. Mechanosensitive ion channel Piezo2 is important for enterochromaffin cell response to mechanical forces. J Physiol. 2017;595:79–91.
43. Zeng WZ, Marshall KL, Min S, Daou I, Chapleau MW, Abboud FM, Liberles SD, Patapoutian A. PIEZOs mediate neuronal sensing of blood pressure and the baroreceptor reflex. Science. 2018;362:464–7.
44. Coste B, Xiao B, Santos JS, Syeda R, Grandl J, Spencer KS, Kim SE, Schmidt M, Mathur J, Dubin AE, et al. Piezo proteins are pore-forming subunits of mechanically activated channels. Nature. 2012;483:176–81.
45. Coste B, Mathur J, Schmidt M, Earley TJ, Ranade S, Petrus MJ, Dubin AE, Patapoutian A. Piezo1 and Piezo2 are essential components of distinct mechanically activated cation channels. Science. 2010;330:55–60.
46. Ge J, Li W, Zhao Q, Li N, Chen M, Zhi P, Li R, Gao N, Xiao B, Yang M. Architecture of the mammalian mechanosensitive Piezo1 channel. Nature. 2015;527:64–9.
47. Cahalan SM, Lukacs V, Ranade SS, Chien S, Bandell M, Patapoutian A. Piezo1 links mechanical forces to red blood cell volume. Elife. 2015; 4.
48. Woo SH, Ranade S, Weyer AD, Dubin AE, Baba Y, Qiu Z, Petrus M, Miyamoto T, Reddy K, Lumpkin EA, et al. Piezo2 is required for Merkel-cell mechanotransduction. Nature. 2014;509:622–6.
49. Ranade SS, Woo SH, Dubin AE, Moshourab RA, Wetzel C, Petrus M, Mathur J, Bégay V, Coste B, Mainquist J, et al. Piezo2 is the major transducer of mechanical forces for touch sensation in mice. Nature. 2014;516:121–5.
50. Feng J, Luo J, Yang P, Du J, Kim BS, Hu H. Piezo2 channel-Merkel cell signaling modulates the conversion of touch to itch. Science. 2018;360:530–3.
51. Gonçalves AN, Correia-Pinto J, Nogueira-Silva C. ROBO2 signaling in lung development regulates SOX2/SOX9 balance, branching morphogenesis and is dysregulated in nitrofen-induced congenital diaphragmatic hernia. Respir Res. 2020;21:302.
52. Nemeth EF, Steffey ME, Hammerland LG, Hung BC, Van Wagenen BC, DelMar EG, Balandrin MF. Calcimimetics with potent and selective activity on the parathyroid calcium receptor. Proc Natl Acad Sci USA. 1998;95:4040–5.
53. Ma T, Thiagarajah JR, Yang H, Sonawane ND, Folli C, Galietta LJ, Verkman AS. Thiazolidinone CFTR inhibitor identified by high-throughput screening blocks cholera toxin-induced intestinal fluid secretion. J Clin Invest. 2002;110:1651–8.
54. Raimondo JV, Joyce B, Kay L, Schlagheck T, Newey SE, Srinivas S, Akerman CJ. A genetically-encoded chloride and pH sensor for dissociating ion dynamics in the nervous system. Front Cell Neurosci. 2013;7:202.
55. Gnanasambandam R, Ghatak C, Yasmann A, Nishizawa K, Sachs F, Ladokhin AS, Sukharev SI, Suchyna TM. GsMTx4: mechanism of inhibiting mechanosensitive ion channels. Biophys J. 2017;112:31–45.
56. Maneshi MM, Ziegler L, Sachs F, Hua SZ, Gottlieb PA. Enantiomeric Aβ peptides inhibit the fluid shear stress response of PIEZO1. Sci Rep. 2018;8:14267.
57. Massoud EA, Sekhon HS, Rotschild A, Puterman ML, Matsui R, Thurlbeck WM. In vitro branching morphogenesis of the fetal rat lung. Pediatr Pulmonol. 1993;15:89–97.
58. Bajanca F, Luz M, Duxson MJ, Thorsteinsdottir S. Integrins in the mouse myotome: developmental changes and differences between the epaxial and hypaxial lineage. Dev Dyn. 2004;231:402–15.
59. Lazarus A, Del-Moral PM, Ilovich O, Mishani E, Warburton D, Keshet E. A perfusion-independent role of blood vessels in determining branching stereotypy of lung airways. Development. 2011;138:2359–68.
60. Alcorn D, Adamson TM, Lambert TF, Maloney JE, Ritchie BC, Robinson PM. Morphological effects of chronic tracheal ligation and drainage in the fetal lamb lung. J Anat. 1977;123:649–60.
61. Harding R, Hooper SB. Regulation of lung expansion and lung growth before birth. J Appl Physiol. 1985;1996(81):209–24.
62. Hooper SB, Harding R. Fetal lung liquid: a major determinant of the growth and functional development of the fetal lung. Clin Exp Pharmacol Physiol. 1995;22:235–47.
63. Harding R, Sigger JN, Wickham PJ, Bocking AD. The regulation of flow of pulmonary fluid in fetal sheep. Respir Physiol. 1984;57:47–59.
64. Yeganeh B, Bilodeau C, Post M. Explant culture for studying lung development. Methods Mol Biol. 2018;1752:81–90.

65. Bartoszewski R, Matalon S, Collawn JF. Ion channels of the lung and their role in disease pathogenesis. Am J Physiol Lung Cell Mol Physiol. 2017;313:L859-l872.
66. Solymosi EA, Kaestle-Gembardt SM, Vadász I, Wang L, Neye N, Chupin CJ, Rozowsky S, Ruehl R, Tabuchi A, Schulz H, et al. Chloride transport-driven alveolar fluid secretion is a major contributor to cardiogenic lung edema. Proc Natl Acad Sci USA. 2013;110:E2308-2316.
67. Matalon S, Bartoszewski R, Collawn JF. Role of epithelial sodium channels in the regulation of lung fluid homeostasis. Am J Physiol Lung Cell Mol Physiol. 2015;309:L1229-1238.
68. Delpire E, Staley KJ. Novel determinants of the neuronal Cl(−) concentration. J Physiol. 2014;592(19):4099–114.
69. Glykys J, Dzhala V, Egawa K, Balena T, Saponjian Y, Kuchibhotla KV, et al. Local impermeant anions establish the neuronal chloride concentration. Science. 2014;343(6171):670–5.
70. Düsterwald KM, Currin CB, Burman RJ, Akerman CJ, Kay AR, Raimondo JV. Biophysical models reveal the relative importance of transporter proteins and impermeant anions in chloride homeostasis. Elife. 2018; 7.
71. Nardo L, Hooper SB, Harding R. Stimulation of lung growth by tracheal obstruction in fetal sheep: relation to luminal pressure and lung liquid volume. Pediatr Res. 1998;43:184–90.
72. Badri KR, Zhou Y, Schuger L. Embryological origin of airway smooth muscle. Proc Am Thorac Soc. 2008;5:4–10.
73. McCray PB Jr, Reenstra WW, Louie E, Johnson J, Bettencourt JD, Bastacky J. Expression of CFTR and presence of cAMP-mediated fluid secretion in human fetal lung. Am J Physiol. 1992;262(4 Pt 1):L472–81.
74. Meyerholz DK, Stoltz DA, Namati E, Ramachandran S, Pezzulo AA, Smith AR, et al. Loss of cystic fibrosis transmembrane conductance regulator function produces abnormalities in tracheal development in neonatal pigs and young children. Am J Respir Crit Care Med. 2010;182(10):1251–61.
75. Bergeron C, Cantin AM. Cystic fibrosis: pathophysiology of lung disease. Semin Respir Crit Care Med. 2019;40(6):715–26.
76. Benedetto R, Ousingsawat J, Wanitchakool P, Zhang Y, Holtzman MJ, Amaral M, et al. Epithelial chloride transport by CFTR requires TMEM16A. Sci Rep. 2017;7(1):12397.
77. Dinsdale RL, Pipatpolkai T, Agostinelli E, Russell AJ, Stansfeld PJ, Tammaro P. An outer-pore gate modulates the pharmacology of the TMEM16A channel. Proc Natl Acad Sci USA. 2021; 118(34)
78. He M, Wu B, Ye W, Le DD, Sinclair AW, Padovano V, Chen Y, Li KX, Sit R, Tan M, et al: Chloride channels regulate differentiation and barrier functions of the mammalian airway. Elife. 2020; 9.
79. Liu Q, Liu K, Cui G, Huang X, Yao S, Guo W, Qin Z, Li Y, Yang R, Pu W, et al. Lung regeneration by multipotent stem cells residing at the bronchioalveolar-duct junction. Nat Genet. 2019;51:728–38.
80. Leslie KO, Mitchell JJ, Woodcock-Mitchell JL, Low RB. Alpha smooth muscle actin expression in developing and adult human lung. Differentiation. 1990;44:143–9.
81. Mailleux AA, Kelly R, Veltmaat JM, De Langhe SP, Zaffran S, Thiery JP, Bellusci S. Fgf10 expression identifies parabronchial smooth muscle cell progenitors and is required for their entry into the smooth muscle cell lineage. Development. 2005;132:2157–66.
82. Shan L, Subramaniam M, Emanuel RL, Degan S, Johnston P, Tefft D, Warburton D, Sunday ME. Centrifugal migration of mesenchymal cells in embryonic lung. Dev Dyn. 2008;237:750–7.
83. Lowey S, Trybus KM. Role of skeletal and smooth muscle myosin light chains. Biophys J. 1995;68:120S-126S (**discussion 126S–127S**).
84. Álvarez-Santos MD, Álvarez-González M, Estrada-Soto S, Bazán-Perkins B. Regulation of myosin light-chain phosphatase activity to generate airway smooth muscle hypercontractility. Front Physiol. 2020;11:701.
85. Yu H, Chakravorty S, Song W, Ferenczi MA. Phosphorylation of the regulatory light chain of myosin in striated muscle: methodological perspectives. Eur Biophys J. 2016;45:779–805.
86. Jesudason EC, Smith NP, Connell MG, Spiller DG, White MR, Fernig DG, Losty PD. Developing rat lung has a sided pacemaker region for morphogenesis-related airway peristalsis. Am J Respir Cell Mol Biol. 2005;32:118–27.
87. Seaborn T, St-Amand J, Cloutier M, Tremblay MG, Maltais F, Dinel S, Moulin V, Khan PA, Piedboeuf B. Identification of cellular processes that are rapidly modulated in response to tracheal occlusion within mice lungs. Pediatr Res. 2008;63:124–30.
88. Benavides F, Rulicke T, Prins JB, Bussell J, Scavizzi F, Cinelli P, Herault Y, Wedekind D. Genetic quality assurance and genetic monitoring of laboratory mice and rats: FELASA Working Group Report. Lab Anim 2019:23677219867719.

Publisher's Note